Phytoplankton life strategies, phenological shifts and climate change in the North Atlantic Ocean from 1850 to 2100

Loïck Kléparski, Grégory Beaugrand, Martin Edwards, Clare Ostle

Phytoplankton life strategies, phenological shifts and climate change in the North Atlantic Ocean from 1850-2100

Loïck Kléparski [1,2], Grégory Beaugrand [1], Martin Edwards[3, 4], Clare Ostle[2]

[1] Univ. Littoral Côte d'Opale, CNRS, Univ. Lille, UMR 8187 - LOG - Laboratoire d'Océanologie et de Géosciences, F-62930 Wimereux, France

[2] Marine Biological Association, Citadel Hill, Plymouth PL1 2PB, United Kingdom.

[3] Plymouth Marine Laboratory, Prospect Place, Plymouth PL13DH, United Kingdom.

[4] University of Plymouth, School of Biological and Marine Sciences, Drake Circus, Plymouth, United Kingdom.

Key-words: diatoms, oblates, prolates, dinoflagellates, phenology, annual phytoplankton succession, climate change

Running title: Phytoplankton life strategies and climate

Abstract

Significant phenological shifts induced by climate change are projected within the phytoplankton community. However, projections from current Earth System Models (ESMs) understandably rely on simplified community responses that do not consider evolutionary strategies manifested as various phenotypes and trait groups. Here, we use a species-based modelling approach, combined with large-scale plankton observations, to investigate past, contemporary and future phenological shifts in diatoms (grouped by their morphological traits) and dinoflagellates in three key areas of the North Atlantic Ocean (North Sea, North-East Atlantic and Labrador Sea) from 1850 to 2100. Our study reveals that the three phytoplanktonic groups exhibit coherent and different shifts in phenology and abundance throughout the North Atlantic Ocean. The seasonal duration of large flattened (i.e., oblate) diatoms is predicted to shrink and their abundance to decline, whereas the phenology of slow-sinking elongated (i.e., prolate) diatoms and of dinoflagellates is expected to expand and their abundance to rise, which may alter carbon export in this important sink region. The increase in prolates and dinoflagellates, two groups currently not considered in ESMs, may alleviate the negative influence of global climate change on oblates, which are responsible of massive peaks of biomass and carbon export in spring. We suggest that including prolates and dinoflagellates in models may improve our understanding of the influence of global climate change on the biological carbon cycle in the oceans.

1. Introduction

Current Earth System Models (ESMs) are projecting a decline in phytoplankton abundance (Bopp et al., 2013; Dutkiewicz et al., 2013; IPCC, 2019; Kwiatkowski et al., 2020) and anticipate significant phenological shifts (Asch et al., 2019; Henson et al., 2013, 2018; Yamaguchi et al., 2022) that may lead to trophic desynchronization and community reorganisation (Edwards & Richardson, 2004; IPCC, 2019; Winder & Schindler, 2004; Yamaguchi et al., 2022). Phenological shifts in phytoplankton are expected because of ocean warming (and also freshening in the poles) and its strengthening influence on water column stability, which is expected to diminish nutrients supply in the euphotic zone, favouring small phytoplankton (e.g., nanoplankton and picoplankton) at the expense of diatoms (Bopp et al., 2005; Marinov et al., 2010), a major group thought to be responsible for 40% of total marine primary production (Field et al., 1998; Tréguer et al., 2018).

Although shifts in phytoplankton phenology are now widely observed among marine and freshwater ecosystems (Friedland et al., 2018; Poloczanska et al., 2013; Thackeray et al., 2016), the examination of diatom seasonality in some regions of the North Atlantic suggests a relative stability (Chivers et al., 2020; Edwards & Richardson, 2004). These unexpected results may originate from the range of strategies that have been developed by diatoms and enable them to occur in diverse environments (Kemp & Villareal, 2013, 2018). Among those strategies, diatom morphological traits might have an important influence on species phenology (Kléparski et al., 2022). Indeed, it has recently been shown that diatom cell shape has evolved as a key adaptation that confers to a species a specific phenology, oblate (i.e., flattened) diatoms being dominant in well-mixed, nutrients-rich, low-stratified waters whereas prolate (i.e., elongated) diatoms dominate in the stratified low-nutrient waters (Kléparski et al., 2022). Cell elongation of prolate diatoms enhances their buoyancy without altering their capacity to absorb nutrients, conferring them a selective advantage in stratified low-nutrient waters (Kléparski et al., 2022).

Most projected phenological shifts (Asch et al., 2019; Henson et al., 2013, 2018; Yamaguchi et al., 2022), which rely on the analyses of variables such as chlorophyll concentration or net primary production, originate from ESMs that only consider a few phytoplankton types (only one for diatoms and none for dinoflagellates). Therefore, those models cannot anticipate subtle changes in phytoplankton community (Kemp & Villareal, 2018; Séférian et al., 2020; Tréguer et al., 2018) and some discrepancies have been reported between satellite observations and model projections (Cabré et al., 2016). Here we applied a species-based modelling approach, combined with large-scale plankton observations, to investigate past, contemporary and future long-term changes (1850-2100) in the phenology of oblates, prolates and dinoflagellates by using six ESMs and two climate warming scenarios (a medium and a high emission scenario, i.e., SSP2-4.5 and SSP5-8.5).

2. Materials and Methods

2.1. Biological data

Phytoplankton data came from the Continuous Plankton Recorder (CPR) survey. The CPR is a long-term plankton monitoring programme that has collected plankton on a monthly basis in the North Atlantic Ocean and its adjacent seas since 1946. The sampling instrument is a high-speed plankton recorder towed behind voluntary merchant ships (called “ships of opportunity”) at a depth of approximately 7m (Beaugrand et al., 2003; Reid et al., 2003). As phytoplankton sampling remained unchanged since 1958

(Warner & Hays, 1994) and historical climatic simulations ended in 2014 (see section 2.2 below), we used the abundance data collected for the diatoms and the dinoflagellates between 1958 and 2014. Each value of abundance corresponds to a number of cells per CPR sample, which corresponds to ~3 m^3 of seawater filtered (Jonas et al., 2004). Species that were first identified after 1958 were discarded from the analyses. In order to account for the climatic variability that was observed in the North Atlantic sector during the period (Beaugrand et al., 2019; Edwards et al., 2002) and minimize the noise associated with the CPR sampling (e.g., exceptional high abundance caused by local hydro-meteorological events, patchiness or abundance misestimation), we calculated a daily mean abundance climatology (based on 365 days) for each species for three 18-year periods: 1958-1976, 1977-1995 and 1996-2014 (a total of 365 days x 3 = 1095 days). The three periods were chosen to be of even length. Therefore, we were able to consider the seasonal signal and the long-term trend, which would have been impossible by using a single climatology based on the entire available time period (Mannocci et al., 2017). Climatologies were estimated in three distinct oceanic regions of the North Atlantic: (i) the North Sea (51°N to 60°N, -3°E to 9°E), (ii) the North-East Atlantic (61°N to 63.5°N, -21°E to -8°E) and (iii) the Labrador Sea (48°N to 60°N, -55°E to -40°E). Climatologies were calculated in a given region for the species/taxa that were present in more than 100 CPR samples. A total of 44 species/taxa were therefore selected (Supplementary Table S1). Climatologies (for the three periods) were smoothed in each region by means of a double 6-order simple moving average (i.e., thirteen-day window) and subsequently standardised between 0 and 1, applying the approach of Caracciolo and colleagues (Caracciolo et al., 2021). Standardisation was performed as follows:

$$A^*_{(i,j)} = \frac{A_{ij}}{max(A_j)} \qquad (1)$$

With $A^*_{(i,j)}$ the standardised abundance of species j on day i, A_{ij} the abundance of species j on day i and $max(A_j)$ the maximal abundance of species j in the three regions (i.e., North Sea, North-East Atlantic and Labrador Sea) between 1958 and 2014. By doing so, the variations in $A^*_{(i,j)}$ reflect both the differences within and between the three regions. We then estimated the 90th percentile of the abundance (P90) of each species using the non-standardised daily climatologies in the three oceanic regions (Supplementary Table S1).

Species were divided into three groups: oblate and prolate diatoms and dinoflagellates, which are known to have distinct environmental requirements (Irwin et al., 2012; Kléparski et al., 2022) (see Supplementary Table S1). The oblate group gathered diatoms (species or taxa) that have a mean cell diameter greater than their mean cell height and the prolate group the diatoms (species or taxa) that have a mean cell diameter smaller than their mean cell height. Information on diatom cell shapes were retrieved from Kléparski *et. al* 2022 (Kléparski et al., 2022) (their Figure 3). Mean monthly abundances between 1958 and 2014 were estimated for each group and in each oceanic region (Figure 1a-i). Data were subsequently smoothed by means of a first-order simple moving average (i.e., three-month smoothing window) and then standardised between 0 and 1 by using the 90th percentile of the monthly abundance of each taxonomic group ($P90_m$):

$$N^*_m = \frac{N_m}{P90_m} \qquad (2)$$

With N_m^* the standardised monthly abundance of a taxonomic group for month m, N_m the monthly abundance for month m and $P90_m$ the 90th percentile of the monthly abundance of the taxonomic group. In rare cases, standardised monthly abundance above 1 were fixed to 1. We chose to use the 90th percentile here instead of the maximum abundance value (as in equation (1)) because the latter would have been too sensitive to outliers that may originate from multiple causes (e.g., exceptional abundance, patchiness or abundance misestimated from only 3m^3 of seawater filtered; see Supplementary Figure S1).

2.2. CMIP6 climate simulations 1850-2100

Species responses to environmental variability was modelled by using three environmental variables known to influence phytoplankton phenology at high latitudes (Beaugrand & Kirby, 2018; Boyce et al., 2017; Caracciolo et al., 2021; Lewandowska & Sommer, 2010; Miller, 2004): i.e., Sea Surface Temperature (SST; °C), Surface Downwelling Shortwave Radiation (SDSR; W m^{-2}) and dissolved nitrate concentration (mol m^{-3}). Climate projections for the three variables originated from the Coupled Model Intercomparison Project Phase 6 (CMIP6)(Eyring et al., 2016) and were obtained from the Earth System Grid Federation (ESGF). We used the Shared Socioeconomic Pathways (SSP) 2-4.5 and 5-8.5 corresponding respectively to a medium and a high radiative forcing by 2100 (4.5 W m^{-2} and 8.5 W m^{-2})(O'Neill et al., 2016, 2017). The simulations of six different ESMs (i.e., CNRM-ESM2-1, GFDL-ESM4, IPSL-CM6A-LR, MPI-ESM1-2-LR, NorESM2-LM and UKESM1-0-LL) covering the time period 1850-2014 (historical simulation) and 2015-2100 (future projections for the two SSP scenarios) were used. An historical perspective is important to better understand the magnitude of the present and future shifts (Beaugrand et al., 2015). The six ESMs were chosen on the basis of data availability for 1850-2100 and the two warming scenarios. All the data were interpolated into daily on a 0.5° by 0.5° regular grid. Key references (i.e., DOI and dataset version) are provided in Supplementary Text S1. Long-term projected changes of the three variables, for the six models, the two scenarios and the three regions are displayed in Supplementary Figures S2-4.

2.3. The MacroEcological Theory on the Arrangement of Life (METAL)

A framework from the METAL theory was used to investigate past, contemporary and future phenological changes of the three taxonomic groups. METAL is a theory that attempts to explain how biodiversity, from the individual to the community level, is organised in space and time and how it responds to environmental changes (Beaugrand, 2015). Based on the concept of the ecological niche *sensu* Hutchinson (i.e., the set of conditions enabling a species to growth and reproduce)(Hutchinson, 1957), one fundamental assumption of METAL is that the niche-environment interaction is a fundamental interaction that enables one to unify and predict a large number of ecological and biogeographical phenomena, as well as the effect of climate-induced environmental changes on individuals, species and communities (Beaugrand, 2015; Beaugrand & Kirby, 2016, 2018). Recently, it has been shown that a framework originating from METAL and using the data collected by the CPR survey, could also explain phytoplankton phenology and the resulting annual plankton succession in the North Sea, based on SST, SDSR and nitrate concentration (Caracciolo et al., 2021). By creating a local pseudo-community, composed of fictive species (i.e., pseudo-species), it was possible to reconstruct at a species level phytoplankton phenology and at a community level the annual plankton succession (Caracciolo et al., 2021). We therefore applied the same framework here to explore how

diatom (oblate and prolate) and dinoflagellate phenology might be modified in the coming decades with global climate change.

2.4. Niches characterisation

We first estimated daily climatologies (based on 365 days) of the three environmental variables described above (i.e., SST, SDSR and nitrate concentration) for three time periods (1958-1976, 1977-1995 and 1996-2014 i.e., 365 days x 3 = 1095 days), three oceanic regions (North Sea, North-East Atlantic and Labrador Sea) and based on six ESMs (i.e., CNRM-ESM2-1, GFDL-ESM4, IPSL-CM6A-LR, MPI-ESM1-2-LR, NorESM2-LM and UKESM1-0-LL). The daily climatologies were then visually compared against the observations originating from the ERA5 dataset (for SST and SDSR; https://cds.climate.copernicus.eu/cdsapp#!/dataset/reanalysis-era5-pressure-levels?tab=overview) and the World Ocean Atlas (for nitrate concentration; https://www.ncei.noaa.gov/products/world-ocean-atlas). For SST and SDSR, because of data availability, daily means were estimated in the three regions between 1959 and 2014 and then converted into daily climatologies for the three time periods (1959-1976, 1977-1995 and 1996-2014). For nitrate concentration, a monthly climatology for the time period 1955-2017 was downloaded from the World Ocean Atlas and a mean was then calculated over the three oceanic regions. Comparisons between observed and reconstructed climatologies from the six ESMs in the North Sea, the North-East Atlantic and the Labrador Sea are displayed in Supplementary Figures S5, S6 and S7 respectively.

Then, we generated a set of 1,755,000 pseudo-species (i.e., fictive species) and we calculated their abundance along the daily climatologies by using a three-dimensional Gaussian niche (Caracciolo et al., 2021):

$$B = ce^{-\frac{1}{2}\left[\left(\frac{x_1 - x_{opt}}{t_1}\right)^2 + \ldots + \left(\frac{x_n - x_{optn}}{t_n}\right)^2\right]} \quad (3)$$

With B the abundance of a pseudo-species along a given environmental gradient x, c the maximum abundance of a pseudo-species (here c was fixed to 1), x_1 to x_n the environmental gradients, with n=3 (SST, SDSR and nitrate concentration). x_{opt1} to x_{optn} are the ecological niche optima along $x_1$to x_n and t_1 to t_n the niche amplitude along $x_1$to x_n. Niche optima were defined for SST from 0 to 25°C every 1°C, for SDSR from 0 to 400 W m^{-2} every 40 W m^{-2} and for nitrate concentration from 0.001 to 0.05 mol m^{-3} every 0.005 mol m^{-3}. Niche amplitudes were defined for SST from 1 to 10°C every 2°C and for nitrate concentration from 0.001 to 0.015 mol m^{-3} every 0.001 mol.m^{-3}. Amplitude for SDSR were defined as followed: 1, 3, 5, 8, 10, 15, 20, 50 and 100 W m^{-2}. Each pseudo-species was therefore defined by a unique combination of optima and amplitudes along the three environmental gradient, i.e., by a unique niche, according to the principle of competitive exclusion (Gause, 1934; Hutchinson, 1978). Therefore, the total number of pseudo-species (1,755,000) corresponds to the total number of unique combinations. Niche intervals were chosen to optimise computational cost while covering the largest set of combinations.

We compared the modelled and observed (CPR) abundance at a species and a group (oblates, prolates and dinoflagellates) level. At a species level, we calculated the Mean Absolute Error (MAE) between the daily abundance climatology (based on 365 days x 3 temporal periods = 1095 days) of each species

and each of the 1,755,000 pseudo-species we created, for each oceanic region and ESM. Some species exhibited erratic short peaks that were difficult to explain in some regions. To prevent our model to be influenced by these events that might be related to misidentification, CPR silk contamination or species expatriation (i.e. species occurring in unsuitable environmental conditions because of their passive drift induced by oceanic currents) (Pulliam, 2000; van der Spoel, 1994), we only summed MAEs from the regions where a given species had a standardised abundance greater than 0.1 during more than 90 days. The use of different thresholds did not alter our conclusions substantially. Finally, for each ESM, we chose a pseudo-species to represent an observed species when it has the lowest MAE in the three regions (Figure 2a-c and Supplementary Table S2). Therefore, the 44 species may be characterised by different pseudo-species from one ESM to another. This allowed us to examine inter-ESM variability (Supplementary Figures S2-7) and the uncertainty associated with the characterisation of a species niche but also to create a unique bias correction for each ESM. Relationships between modelled and observed daily abundance species climatologies in each region were examined by means of a Spearman rank correlation (Figure 2d-f and Supplementary Tables S3-S5).

In order to assess whether the use of climatologies based on three temporal periods (1958-1976, 1977-1995 and 1996-2014) might influence model skill and performance, we also estimated the MAEs between the observed and modelled daily abundance climatologies based on a single (1958-2014) and two temporal periods (1958-1985 and 1986-2014) (Supplementary Figures S8-S9).

2.5. Long-term changes in the abundance of the three taxonomic groups

Daily abundances of the 44 species were estimated from Equation 3 between 1850 and 2100, using environmental variables assessed from the six models and for the two scenarios (Section 2.4 above). To assess the mean abundance of each group, we weighted species abundance by using their P90 (Section 2.1 and Supplementary Table S1) to account for species contemporary difference in abundance within the three groups (oblates, prolates, and dinoflagellates). We used the 90th percentile instead of the maximum abundance value because the latter would have been too sensitive to outliers that may originate from multiple causes (e.g., exceptional abundance, patchiness or abundance misestimated from only 3m^3 of seawater filtered). Predicted abundances were finally standardised between 0 (the lowest abundance) and 1 (the highest) for each taxonomic group, all ESMs and scenarios as follows (Figures 4b-g, 5b-g and 6b-g-):

$$D_m^* = \frac{D_{(m)} - min(D)}{max(D) - min(D)} \qquad (4)$$

With D_m^* the standardised predicted abundance of a group for a given ESM, scenario and month m, D_m the predicted abundance for month m and $min(D)$ and $max(D)$ the minimal and maximal predicted abundance between 1850 and 2100 in a given oceanic region, respectively. Finally, the relationships between modelled and observed standardised monthly abundances were quantified for 1958-2014 (i.e., overlapping period of observed and modelled data) by using the Spearman correlation coefficient (Figure 1a-r and Table 1). Differences between observed and modelled standardised monthly abundances were also calculated to compare the seasonal and long-term trends (Figure 1s-α).

To test whether the long-term changes in phenology and abundance of the three groups were well modelled by our approach, we also estimated the annual (long-term changes) and monthly (seasonal variations) average of the modelled and observed abundances of the three groups in the three regions, between 1958 and 2014 (Supplementary Figures S10-11). Annual and monthly patterns were subsequently compared by means of a Spearman rank correlation coefficient (Supplementary Tables S6-7).

2.6. Long-term phenological changes of the three taxonomic groups.

We examined phenological shifts of the three taxonomic groups between 1850 and 2100, for the two scenarios and the six ESMs in the three regions. Average daily abundances of each group were smoothed by means of a 15-order moving average (i.e., time scale covering a month) and then, for each year between 1850 and 2100, we estimated six phenological indices: i.e., (1) Maximum Annual Abundance (MAA), (2) the day where MAA is reached, (3) initiation and (4) termination of the Seasonal Reproductive Period (SRP), i.e., the first and the last days where the abundance is ≥50% of MAA, (5) seasonal duration, i.e., the number of consecutive days where abundance is ≥ 50% of MAA, and (6) Integrated Mean Annual Abundance (IMAA) (Figure 3). The six indices were calculated for each taxonomic group, all models, scenarios and North Atlantic regions. Bimodality (i.e., two population peaks within a single year) was sometimes observed for the diatoms in the three regions, but as this pattern fluctuated in time (i.e. short erratic peaks) and was not well reproduced by all ESMs, when a bimodality was observed we only considered the peak with the highest abundance. An average of the results of the six ESMs was then calculated for 1850-2100 for each scenario and North Atlantic region (Figures 4-6). In addition, we focussed on three decades: 1850-1859, 2000-2009 and 2090-2099. For these decades, we assessed the inter-model average and the associated standard deviation of each index (mean ± uncertainty; Supplementary Tables S8-16)(Kwiatkowski et al., 2020).

3. Results

Visual comparisons between observed and reconstructed SST, SDSR and nitrate concentration showed that the seasonal cycle and the long-term trend of each variable was in general well reconstructed by the ESMs in the three oceanic regions and for the three time periods (except for nitrate long-term trend, see Materials and Method and Supplementary Figures S5, S6 and S7).

3.1. Model performances

Model performance was first assessed by visually comparing the observed and modelled daily abundance of each species for the three periods and North Atlantic regions (Supplementary Animation S1-3). The phenology of most species was well modelled by our approach and the Mean Absolute Error (MAE) between the observed and modelled abundance was generally low (below 0.1 for diatoms and below 0.2 for dinoflagellates; Figure 2a-c and Supplementary Table S2; see Materials and Methods). MAEs calculated between observed and modelled abundance based on a single (1958-2014) or two temporal periods (1958-1985 and 1986-2014) climatologies were higher, indicating that our model performed better when based on the three temporal periods climatologies (Supplementary Figures S8 and S9). We then estimated the Spearman rank correlation coefficient between daily observed and modelled patterns, which revealed that for most species, correlations were highly positive (Figure 2d-

f and Supplementary Tables S3-S5). A few low correlations were observed, however, indicating that for some species our approach did not work well in some North Atlantic regions and for some ESMs. Low correlations between observations and model reconstructions may be caused by some regional hydro-meteorological events that are not well reproduced by an ESM or by some methodological limitations of our approach (see Discussion). However, their weight in the subsequent analyses was low, as shown by the value of their P90 (i.e., the 90^{th} percentile of their abundance, Materials and Methods, Figure 2d-f and Supplementary Table S1); the higher the P90, the higher the abundance of a species in a North Atlantic region and therefore the greater its weight in subsequent analyses at the group level (Figure 4-6).

Modelled species abundances were finally aggregated at a monthly scale for each group (oblates, prolates and dinoflagellates) by weighting the abundance of each species according to the value of their P90 (Supplementary Table S1). A monthly scale was first chosen for comparison of the modelling approach with the *in situ* monthly observations collected by the CPR survey, whom sampling is carried out at a monthly interval (Richardson et al., 2006). Differences between observed and modelled long-term changes in monthly abundance showed that model performance varied greatly among regions and species groups, mostly because of the nature of the CPR data (i.e., large variability in observed abundance; see Figure 1a-i versus 1j-r and Discussion) and because the reconstructed climatic variability was not supposed to exactly match the variability that was observed between 1958 and 2014 (Stock et al., 2011). On the contrary, Spearman rank correlations calculated between observed and modelled mean monthly abundances were all positively correlated significantly, although the correlations were statistically more significant in the North Sea and the North-East Atlantic than in the Labrador Sea (Spearman rank correlations coefficient between 0.7 and 0.83 in the North Sea, 0.64 and 0.73 in the North-East Atlantic and 0.5 and 0.58 in the Labrador Sea; Figure 1 and Table 1). The comparison between long-term changes in the annual abundance of prolates in the three regions, of oblates in the North-East Atlantic and of oblates and dinoflagellates in the Labrador Sea were globally well reconstructed (Supplementary Figure S10), but the correlations were not always significant, suggesting that some periods and years did not match well (Supplementary Table S6). On the contrary, our model did not fully reconstruct the long-term trends in oblates and dinoflagellates in the North Sea and of dinoflagellates in the North-East Atlantic (Supplementary Figure S10), which was confirmed by Spearman rank correlations (Supplementary Table S6). Such difficulties to explain observed long-term changes in abundance were expected since ESMs are known to have some difficulties to reconstruct high frequency natural variability in climate well (Stock et al., 2011). Finally, the comparison between observed and modelled monthly changes in abundance revealed that the seasonal cycles of the three groups in the three regions were correctly reconstructed (significant Spearman rank correlations above 0.85; Supplementary Figure S11 and Supplementary Table S7).

3.2. Phenological shifts in the North Atlantic

In the North Atlantic Ocean, phenological shifts projected by our models were relatively moderate for 1850-1950 (Figures 4-6). Major changes were expected to occur from the end of 1970s onwards when the rate of ocean warming increased and led to an increase in water column stratification (IPCC, 2019) (see also Supplementary Figures S2-S4). A decline in oblate abundance was generally observed under both scenarios in the three regions, associated with a reduction of their SRP, whereas an increase in

prolate and dinoflagellate abundance was projected, associated with an expansion of their SRP (Figures 4-6). Expectedly, the magnitude of the projected changes in phenology and abundance appeared to be more important under the high warming scenario (Figures 4-6).

3.3. Phenological shifts in the North Sea

In the North Sea (Figure 4a), modelled long-term daily phenological changes exhibited similar patterns for both SSP scenarios, with a shift in the diatom community composition, although changes were highest under SSP5-8.5 (Figure 4b-q). Oblate diatoms are expected to decline, the MAA decreasing from 1671.1 ± 494.7 cells per CPR sample in 1850-1859 to 1176.9 ± 573.2 or 785.1 ± 347.7 cells per CPR sample in 2090-2099 for scenarios SSP2-4.5 and SSP5-8.5, respectively (Figure 4b and e and Supplementary Table S8). In contrast, prolate MAA rose from 302 ± 53.3 cells per CPR sample in 1850-1859 to 360.5 ± 77.5 or 392.6 ± 115.5 cells per CPR sample in 2090-2099 for SSP2-4.5 and SSP5-8.5, respectively (Figure 4c and f and Supplementary Table S9). No significant changes in the duration of the SRP was found for both groups (Figure 4h-i and Supplementary Tables S8-9), although they exhibit an earlier and a later (both initiation and termination) phenology, respectively (Figure 4j-k and m-n and Supplementary Tables S8-9). These phenological shifts were accompanied by a shift in their IMAA, our results suggesting that oblates may experience a strong decrease from 390 ± 92.8 cells per CPR sample in 1850-1859 to 283.8 ± 97.4 or 192 ± 59 cells per CPR sample in 2090-2099 for scenarios SSP2-4.5 and SSP5-8.5, respectively. An opposite pattern is predicted for prolates, although it may be less important (from 122.8 ± 32.7 cells per CPR sample in 1850-1859 to 134.5 ± 18.6 or 148.8 ± 30.1 cells per CPR sample in 2090-2099 for SSP2-4.5 and SSP5-8.5, respectively; Figure 4p-q and Supplementary Tables S8-9).

Modelled changes in dinoflagellates exhibited a phenological expansion. Their MAA remained constant throughout the period, although they decreased at the very end of the century under SSP5-8.5 from 2853.9 ± 336.3 cells per CPR sample in 1850-1859 to 2599.3 ± 553.2 in 2090-2099 (Figure 4d and g and Supplementary Table S10). The duration of their SRP is expected to rise throughout the twenty first century (from a mean of 103 ± 16 days in 1850-1859 to 107 ± 6 days in 2000-2009 and to 127 ± 13 or 143 ± 25 days in 2090-2099 under SSP2-4.5 and SSP5-8.5 respectively; Figure 4h-i and Supplementary Table S10) with both an earlier initiation and a later termination of their SRP (Figure 4l and o and Supplementary Table S10), associated with an increase in their IMAA (Figure 4p-q and Supplementary Table S10).

3.4. Phenological shifts in the North-East Atlantic

In the North-East Atlantic region (Figure 5a), phenological shifts were also predicted by our approach, the magnitude of which depending upon warming intensity (Figure 5b-q). Oblate MAA decreased after the end of the twenties century whereas prolate MAA rose *circa* 2050 under both scenarios (Figure 5b-c and e-f, Supplementary Tables S11-12). Oblates underwent a phenological contraction from 76 ± 22 days in 2000-2009 to 69 ± 14 or 64 ± 15 days in 2090-2099 for SSP2-4.5 and SSP5-8.5, respectively (Figure 5h-i and Supplementary Table S11), accompanied by an earlier initiation in their SRP (Figure 5j and m and Supplementary Table S11). In contrast, prolates exhibited a strong phenological dilatation from 91 ± 6 days in 2000-2009 to 110 ± 11 or 119 ± 22 days in 2090-2099 for scenarios SSP2-4.5 and SSP5-8.5, respectively (Figure 5h-i and Supplementary Table S12), with an earlier initiation and a later

termination of their SRP (Figure 5k and n and Supplementary Table S12). At the end of the century, they reached earlier their MAA in the year, i.e., around day number 204 ± 16 or 197 ± 19 in 2090-2099 for scenarios SSP2-4.5 and SSP5-8.5, respectively, in comparison to day 215 ± 4 in 1850-1859 (Figure 5k and n and Supplementary Table S12). Oblate IMAA remained constant under scenario SSP2-4.5 but decreased under SSP5-8.5. Prolate IMAA slightly increased under both scenarios but remained below the value observed for oblates (Figure 5p-q and Supplementary Tables S11-12).

Dinoflagellates also underwent a phenological expansion, associated with an increase of their MAA throughout the twenty first century (Figure 5d and g and Supplementary Table S13), a longer duration (Figure 5h-i and Supplementary Table S13) caused by an earlier initiation (around day number 215 ± 4 in 1850-1859 and 204 ± 16 or 197 ± 19 for SSP2-4.5 and 5-8.5, respectively) and a later termination (around day number 254 ± 9 in 1850-1859 and 262 ± 5 or 268 ± 9 in 2090-2099 for scenarios SSP2-4.5 and SSP5-8.5, respectively, Supplementary Table S13) of their SRP. Their IMAA rose above those of oblates during the first half of the twenty first century, although there was a high inter-model variance (Figure 5p-q and Supplementary Table S13).

3.5. Phenological shifts in the Labrador Sea

In the Labrador Sea (Figure 6a), distinct phenological shifts were found, also depending upon the SSP scenarios (Figure 6b-q). Under scenario SSP2-4.5, oblates exhibited a slight increase of their MAA (i.e., 3770.1 ± 769.1 cells per CPR sample in 2000-2009 *versus* 4055.5 ± 545.4 cells per CPR sample in 2090-2099; Supplementary Table S14) although the duration of their SRP slightly diminished from 87 ± 11 days in 2000-2009 to 84 ± 13 days in 2090-2099 (Figure 6h and j and Supplementary Table S14). Prolates maintained both their MAA and IMAA throughout the period 1850-2100 (Figure 6c and p and Supplementary Table S15), the most significant changes occurring in the duration of their SRP (from 97 ± 31 days in 2000-2009 to 107 ± 36 in 2090-2099; Figure 6h and Supplementary Table S15) accompanied by an earlier phenology (Figure 6k and Supplementary Table S15). Dinoflagellates should exhibit a large increase of their MAA, especially after 2050, from 910 ± 428.4 cells per CPR sample in 2000-2009 to 1914.4 ± 1125.2 in 2090-2099 (Figure 6d and Supplementary Table S16) without a significant increase in the duration of their SRP (Figure 6h and Supplementary Table S16) or a change in initiation or termination (Figure 6l and Supplementary Table S16). Their IMAA slightly increased but remained above that of oblates (Figure 6p and Supplementary Tables S14 and 16).

Under SSP5-8.5, our approach predicted a shift from a system dominated by oblates to a system dominated by dinoflagellates (Figure 6b-q). The oblates exhibited a decrease of their MAA from 3770.1 ± 769.1 cells per CPR sample in 2000-2009 to 3184.4 ± 727.2 in 2090-2099 (Figure 6e and Supplementary Table S14), accompanied by a decrease in the duration of their SRP from 86.9 ± 10.5 days in 2000-2009 to 72.8 ± 8.3 days in 2090-2099 (Figure 6i and Supplementary Table S14), and an earlier initiation (Figure 6m and Supplementary Table S14). Their IMAA sharply decreased, especially during the second half of the twenty first century, from 1077.1 ± 178.6 cells per CPR sample in 2000-2009 to 777.9 ± 245.5 in 2090-2099 (Figure 6q and Supplementary Table S14). No changes were found for prolate MAA (Figure 6f and Supplementary Table S15) but their SRP lasted longer, from 97 ± 31 days in 2000-2009 to 115 ± 35 in 2090-2099 (Figure 6i and n and Supplementary Table S15). Their IMAA was low under this scenario (Figure 6p-q and Supplementary Table S15). Dinoflagellate shifts were amplified, their MAA increased substantially, from 910 ± 428.4 cells per CPR sample in 2000-2009 to

2898.2 ± 1052.0 in 2090-2099 (Figure 6g and Supplementary Table S16). These changes were more prominent at the end of the twenty first century, from 66 ± 12 days in 2000-2009 to 82 ± 18 in 2090-2099 (Figure 6i and Supplementary Table S16), resulting in a phenological dilatation (Figure 6o and Supplementary Table S16). Their IMAA tripled between the beginning and the end of the twenty first century, from 204.5 ± 66.9 cells per CPR sample in 2000-2009 to 738.8 ± 319.3 in 2090-2099 (Supplementary Table S16), resulting in a shift from oblates to dinoflagellates. As the long-term phenological changes of the three groups were more difficult to reconstruct in this region (Table 1), our predictions should be considered with degree of caution.

4. Discussion

Some discrepancies between modelled and observed abundance indicate that our model may have some limitations (Figure 1, Supplementary Figures S10-11 and Supplementary Animations S1-3). For example, the increase in the abundance of dinoflagellates in the North Sea and the North-East Atlantic, and of oblates in the North Sea, were not captured well by our approach (Figure 1 and Supplementary Figure S10). In the same way, the fit between observed and reconstructed daily abundances varied among the three different temporal periods (Supplementary Animations S1-3). For example, the abundance of *Leptocylindrus danicus* in the North Sea was correctly reconstructed for the temporal periods 1977-1995 and 1996-2014 but not for 1958-1977 (Supplementary Animation S1). These inconsistencies may originate from (i) our framework, (ii) the CPR sampling and (iii) the ESMs.

4.1. Limitations of our approach

In this study, we made a series of choices and assumptions that might have affected model performance. First, we used an approach based on METAL rather than a species distribution model (SDM). This choice was made because we showed previously that METAL correctly reconstructs phytoplankton phenology and annual succession when applied to the CPR data (Caracciolo et al., 2021) while it has been shown that most SDM poorly performed with those data (Brun et al., 2016). In addition, using METAL enables us to convert the monthly CPR observations at a daily scale, which is more adapted (i) to reconstruct/project the long-term phenological changes from 1850 to 2100, (ii) to examine their trends (Henson et al., 2018) and (iii) to demonstrate that the niche-environment interaction governs long-term phenological phytoplankton shifts (Beaugrand & Kirby, 2018).

Second, we used a symmetric gaussian function to model the thermal niche of the 44 phytoplanktonic species. Phytoplankton are ectotherms and may therefore have asymmetric thermal niches (Martin & Huey, 2008; Thomas et al., 2012); in particular they might be able to tolerate a larger range of cold temperatures (i.e., below their thermal optimum) and a narrower range of warm temperatures (i.e., above their thermal optimum) (Martin & Huey, 2008). However, Caracciolo and colleagues reconstructed phytoplankton phenology and annual succession well in the North Sea by using symmetrical niches (Caracciolo et al., 2021). Furthermore, the use of asymmetrical gaussian functions would have also increased computational cost. Nevertheless, we acknowledge that the consideration of asymmetrical niches might perhaps improve our results. For example, the existence of an upper thermal limit above which the abundance rapidly declined substantially (e.g. the events observed with the dinoflagellates in the North Sea and the North-East Atlantic; Figure 1g-h and Supplementary

Figures S10c and f) was not reproduced by our model; indeed the modelled shifts were almost always gradual (Figure 1p-q and Supplementary Figure S10c and f).

Last, we supposed that species niches will be conserved over the time period 1850-2100 (i.e., the assumption of niche conservatism), an assumption that is generally formulated by modellers that project species response to climate change (Soberon & Nakamura, 2009). The large population size and fast generation time of phytoplankton are supposed to allow a rapid alteration of their niches (Litchman et al., 2012) but some studies (on zooplankton however) have not seen any niche alteration at a decadal scale (Helaouët & Beaugrand, 2007) and there must exist fundamental constraints that limit adaptation (for example, phytoplankton morphological traits, which affect nutrient uptake, are supposed to be highly conserved) (Beaugrand & Kirby, 2018; Kléparski et al., 2022; Litchman et al., 2007).

4.2. Limitations related to the CPR sampling

Another source of discrepancy between modelled and observed abundance may originate from the sampling by the CPR. First, sampling is carried out at a monthly scale over large areas (Richardson et al., 2006) and it is likely that such a sampling frequency is not always appropriate to properly characterise blooms as phytoplankton exhibits typically a short life cycle. Second, the CPR machine uses a 270µm mesh silk that mostly collects large armoured dinoflagellates and chain forming diatoms but undersamples smaller phytoplankton species. These sampling biases might explain the large variability observed in the abundance of phytoplankton species, affecting subsequently niche characterisation and modelled reconstructions (Figure 1a-i). However, our results suggest this is not the case for the vast majority of species (Supplementary Animations S1-3 and Supplementary Tables S2-S5). For example, some of the smallest species, e.g. *Thalassionema nitzschioides* and *Cylindrotheca closterium*, are well modelled in the North Sea and the North-East Atlantic but not in the Labrador Sea (Supplementary Tables S3-S5 and Supplementary Animations S1-S3) suggesting that the problem might not be related with a sampling bias affecting model performance. Third, the CPR sampling is heterogeneous in space and time and some regions were not continuously sampled between 1958 and 2014 (Richardson et al., 2006). For example, no CPR sample was available in the Labrador Sea at the end of the 1980s (white bands in Figure 1c, f, i, u, x and α). However, it is thought that the CPR collects an important fraction of the abundance of each taxon and is therefore though to be robust to examine seasonal and interannual patterns (Richardson et al., 2006).

4.3. Limitations from ESMs

The reconstructed regional climatic variability between 1958 and 2014 by ESMs is not supposed to exactly match the variability that was observed during that time (Stock et al., 2011), a bias that might have also affected niche estimates and that might therefore explain the discrepancies between observed and modelled mean long-term changes in abundance (Figure 1a-r and Supplementary Figure S10). For example, the abundance of *Cylindrotheca closterium* is well modelled in the North Sea with CNRM-ESM2-1, IPSL-CM6A-LR and NorESM2-LM but not with MPI-ESM1-2-LR, GFDL-ESM4 and UKESM1-0-LL (Supplementary Table S3). Indeed, there exists large variations in SST, SDSR and nitrate concentration among the six ESMs in some regions (Supplementary Figures S5-7). Nevertheless, it should be noticed that our approach consistently modelled the seasonal cycle of the three groups in

the three regions and the modelled long-term trends were generally in agreement with the observations, especially for prolates in the three regions, oblates in the North-East Atlantic and oblates and dinoflagellates in the Labrador Sea (Supplementary Figures S10-11 and Supplementary Tables S6-7).

4.4. Long-term changes in the phenology of diatoms and dinoflagellates

Modelled shifts are in agreement with theoretical projections, i.e., that spring species (i.e., oblates) experience a phenological contraction and an earlier phenology whereas late summer species (i.e., prolates and dinoflagellates) exhibit a phenological expansion with both an earlier initiation and a later termination (Beaugrand & Kirby, 2018). The phenological contraction of oblates, associated with a decline in abundance, is indicative of species/taxa that reach the limits of their phenological plasticity (Beaugrand & Kirby, 2018), probably because an earlier phenology in spring is impossible as winter photoperiod and light levels limits primary production at high latitudes (Boyce et al., 2017; Caracciolo et al., 2021) and/or because the decrease in nitrate concentration (Supplementary Figures S2-4), which are an essential constituent of proteins and nucleic acids that are in turn critical for the synthesis of organic matter (Miller, 2004), limits the size of the bloom. Therefore, these diatoms might encounter more favourable environmental conditions at high latitudes, causing a biogeographical shift, a postulate that would be in agreement with the increased primary production projected by ESMs in the Arctic region (Kwiatkowski et al., 2020) and the observed increase and decrease of diatom populations in the North-Sea and the bay of Biscay, respectively (Edwards et al., 2022). On the contrary, the phenological expansion of prolates and dinoflagellates is indicative of species/taxa that are adapted to the reinforced stratified and nutrient-depleted conditions in the future North Atlantic Ocean (Beaugrand & Kirby, 2018; Kwiatkowski et al., 2020). The elongated cell shape of prolates reduces their sinking speed while not affecting their capacity to uptake nutrients, enabling them to remain in the well-lit upper part of the water column (Kléparski et al., 2022; Padisak et al., 2003). Furthermore, it has been shown that some taxa belonging to this taxonomic group (e.g., *Rhizosolenia*), were able to passively migrate between the surface layers and the nutricline, enabling them to harvest nutrients more efficiently (Kemp & Villareal, 2013, 2018). Similarly, the dinoflagellates have flagella which enable them to move and actively exploit nutrients in the water column. They are also capable of switching nutritional strategies to mixotrophy when less nutrients are available (Miller, 2004).

Because of the shifts in phytoplankton phenology, changes in species succession are expected to desynchronise species interaction and trigger trophic mismatch (Beaugrand et al., 2003; Edwards & Richardson, 2004). Mismatch may occur between species that have different range of tolerance along a single environmental variable. Such alterations of the trophodynamics have already been observed in freshwater lakes (Winder & Schindler, 2004) but remain difficult to anticipate in the marine environment because each species has a specific response to environmental variability, which is driven by its life strategy and its niche (Beaugrand & Kirby, 2018). Furthermore, it has also been shown that only seasonally heterogeneous environmental changes can lead to a desynchronization in species interaction (e.g., warmer temperature in spring but not in summer)(Straile et al., 2015). Results from the METAL theory suggest that trophic mismatch might be limited however, because interacting species have at least a part of their ecological niche in common, providing that no other important ecological dimensions or habitat requirements differ among them (Beaugrand & Kirby, 2018). Indeed, species are more expected to track changes along the environmental variables for which they have the

narrowest tolerance (Ackerly, 2003). Therefore, in the pelagic environment, one could expect a mismatch among species that are not linked to the same habitat components (i.e., the stable- and substrate-biotope components) (van der Spoel, 1994). For example, it has been shown that a shift in phytoplankton phenology is more likely to affect the fish that spawn in geographically fixed areas rather than those that have their spawning grounds moving according to the environmental changes (Asch et al., 2019).

Diatoms and dinoflagellates have been historically separated into two distinct functional types (Kemp & Villareal, 2018; Margalef, 1978). According to Margalef's mandala (Margalef, 1978), diatoms thrive when the water column is poorly stratified and turbulent and when nutrients concentration is relatively high. In contrast, dinoflagellates dominate in stratified conditions and lower nutrients concentration. By simplifying Margalef's framework (Margalef, 1978), a decline in primary production and carbon export (therefore the biological pump (Passow & Carlson, 2012)) is anticipated in the North Atlantic because ocean warming will enhance water column stratification and reduce nutrients, which are believed to negatively affect the diatoms as a whole (Bopp et al., 2005; Kemp & Villareal, 2018; Kléparski et al., 2022; Marinov et al., 2010; Tréguer et al., 2018). Our results nuance these projections. Although they show that diatom abundance as a whole will decrease, they also suggest that prolates may indeed persist and increase in a more stratified ocean, albeit probably not to an abundance level that might compensate the large diminution in the abundance experienced by oblates. Indeed, massive blooms of those last diatoms in spring generate high carbon export through the generation of marine snow (Kléparski et al., 2022; Raven & Waite, 2004; Smetacek, 1985) and it is therefore unlikely that the slight increase in prolates will overcome the decrease in carbon exportation induced by the reduction in oblate abundance. Furthermore, the transfer efficiency of carbon to the deep ocean is reduced with smaller sized slow-sinking cells, and therefore the shift from large round oblates to smaller elongated prolates will also diminish the rate of carbon export (Henson et al., 2022). Whether this shift might also affect species aggregation remains an open question as the causes of this phenomenon are not clear (e.g., defence against predation, response to changes in turbulence or buoyancy regulation) (Lürling, 2021; Pančić & Kiørboe, 2018; Smayda, 1970; Sournia, 1982). Our results also suggest that dinoflagellate abundance will rise in the three North Atlantic regions. Although the contribution of this group to the biological pump is poorly understood, a study has shown that dinoflagellate blooms sometimes coincide with a rise in carbon export at an annual scale in the North-East Atlantic at 3000m (Henson et al., 2012). It has also been shown that the consideration of mixotrophic organisms (e.g., dinoflagellates) within biogeochemical models can increase the flux of carbon export (Ward & Follows, 2016). Therefore, this group might alleviate to some extent the consequences of the reduction in oblates on the biological pump in the North Atlantic, albeit export from the surface ocean is also strongly influenced by synergistic effects such as nutrient delivery through remineralisation or direct inputs, processes that are difficult to predict (Passow & Carlson, 2012).

ESMs used as part of CMIP5 included a few functional types to represent the phytoplanktonic community, often with a single grouping for diatoms (Séférian et al., 2020; Tréguer et al., 2018). The last generations of ESMs in CMIP6 have improved the representation of phytoplankton ecology by including more functional types (e.g., diazotrophs for some models), which has enhanced model performance. However, diatoms still remain represented by a single group (Séférian et al., 2020). Results from model inter-comparisons highlight the great sensitivity of models to the types of functional groups they include, as well as the ecological traits they represent (Fu et al., 2016; Taucher

& Oschlies, 2011). Dutkiewicz and colleagues have recently used morphological traits (i.e., cell size), biogeochemical functions and thermal tolerances to define more than 350 phytoplankton types (Dutkiewicz et al., 2020). Their results showed that species richness projections were altered by the number as well as the nature of phytoplankton traits, each controlling a distinct aspect of the species' responses (Dutkiewicz et al., 2020). They concluded that the addition of traits, such as cell shape, might improve model projections (Dutkiewicz et al., 2020). *In situ* studies have also highlighted the importance of phytoplankton composition for carbon exportation (Dybwad et al., 2021; Henson et al., 2012). However, such models with hundreds of phytoplankton types cannot realistically be used to perform centennial climatic simulations because of computational cost. Hence, although our results with oblates give some support to the ESMs that only considered a single diatom group, they also emphasize that prolates and dinoflagellates exhibit distinct alterations of their phenology and abundance. Therefore, the distinction of oblate and prolate diatoms as well as dinoflagellates in ESM models may be a simple way to improve model projections because these three groups have different phenologies and responses to climate change, which may affect our current understanding of the consequences of phytoplankton shifts on the biological carbon pump (Karp-Boss & Boss, 2016; Kléparski et al., 2022; Litchman & Klausmeier, 2008; Naselli-Flores et al., 2021; Ryabov et al., 2020).

Acknowledgments:

We acknowledge the World Climate Research Programme, which, through its Working Group on Coupled Modelling, coordinated and promoted CMIP6. We thank the climate modelling groups for producing and making available their model output, the Earth System Grid Federation (ESGF) for archiving the data and providing access, and the multiple funding agencies who support CMIP6 and ESGF. We also thank the owners and crews that have towed the CPRs on a voluntary basis for over 80 years contributing to one of the world's largest and longest ongoing ecological experiments. Without these early pioneers of citizen science and broad-scale volunteer monitoring projects this unique ecological dataset would never have been financially or logistically viable.

Funding:

Funding that supports data collection has come from a number of contracts since inception of the Continuous Plankton Recorder survey, the current funded projects include: the UK Natural Environment Research Council, Grant/Award Number: NE/R002738/1 and NE/M007855/1; EMFF; Climate Linked Atlantic Sector Science, Grant/Award Number: NE/ R015953/1, DEFRA UK ME-5308, NSF USA OCE-1657887, DFO CA F5955- 150026/001/HAL, NERC UK NC-R8/H12/100, Horizon 2020: 862428 Atlantic Mission and AtlantECO 862923, IMR Norway, DTU Aqua Denmark and the French Ministry of Environment, Energy, and the Sea (MEEM). This work was also financially supported by the European Union, European Regional Development Fund (ERDF), the French State, the French Region Hauts-de-France and Ifremer, in the framework of the project CPER IDEAL 2021–2027. LK also received funds as part of a PhD grant co-financed by the French Region Hauts de France region and the Marine Biological Association.

Data accessibility:

All the data used in this article are already freely available (see the Materials and Methods section and Supplementary Text S1).

Author contributions: L.K and G.B designed the study, performed the analyses and wrote the first draft. L.K, G.B, M.E and C.O discussed the results and reviewed the manuscript.

Conflict of interest: The authors declare no conflict of interest.

References

Ackerly, D. D. (2003). Community Assembly, Niche Conservatism, and Adaptive Evolution in Changing Environments. *International Journal of Plant Sciences*, *164*(S3), S165–S184. https://doi.org/10.1086/368401

Asch, R. G., Stock, C. A., & Sarmiento, J. L. (2019). Climate change impacts on mismatches between phytoplankton blooms and fish spawning phenology. *Global Change Biology*, *25*(8), 2544–2559. https://doi.org/10.1111/gcb.14650

Beaugrand, G. (2015). *Marine biodiversity, climatic variability and Global Change*. Routledge.

Beaugrand, G., Brander, K. M., Lindley, J. A., Souissi, S., & Reid, P. C. (2003). Plankton effect on cod recruitment in the North Sea. *Nature*, *426*(6967), 661–664. https://doi.org/10.1038/nature02164

Beaugrand, G., Conversi, A., Atkinson, A., Cloern, J., Chiba, S., Fonda-Umani, S., Kirby, R. R., Greene, C., Goberville, E., Otto, S. A., Reid, P. C., Stemmann, L., & Edwards, M. (2019). Prediction of unprecedented biological shifts in the global ocean. *Nature Climate Change*, *9*, 10.

Beaugrand, G., Edwards, M., Raybaud, V., Goberville, E., & Kirby, R. R. (2015). Future vulnerability of marine biodiversity compared with contemporary and past changes. *Nature Climate Change*, *5*(7), 695–701. https://doi.org/10.1038/nclimate2650

Beaugrand, G., & Kirby, R. R. (2016). Quasi-deterministic responses of marine species to climate change. *Climate Research*, *69*(2), 117–128. https://doi.org/10.3354/cr01398

Beaugrand, G., & Kirby, R. R. (2018). How Do Marine Pelagic Species Respond to Climate Change? Theories and Observations. *Annual Review of Marine Science*, *10*(1), 169–197. https://doi.org/10.1146/annurev-marine-121916-063304

Bopp, L., Aumont, O., Cadule, P., Alvain, S., & Gehlen, M. (2005). Response of diatoms distribution to global warming and potential implications: A global model study. *Geophysical Research Letters*, *32*(19), L19606. https://doi.org/10.1029/2005GL023653

Bopp, L., Resplandy, L., Orr, J. C., Doney, S. C., Dunne, J. P., Gehlen, M., Halloran, P., Heinze, C., Ilyina, T., Séférian, R., Tjiputra, J., & Vichi, M. (2013). Multiple stressors of ocean ecosystems in the 21st century: Projections with CMIP5 models. *Biogeosciences*, *10*(10), 6225–6245. https://doi.org/10.5194/bg-10-6225-2013

Boyce, D. G., Petrie, B., Frank, K. T., Worm, B., & Leggett, W. C. (2017). Environmental structuring of marine plankton phenology. *Nature Ecology & Evolution*, *1*(10), 1484–1494. https://doi.org/10.1038/s41559-017-0287-3

Brun, P., Kiørboe, T., Licandro, P., & Payne, M. R. (2016). The predictive skill of species distribution models for plankton in a changing climate. *Global Change Biology*, *22*(9), 3170–3181. https://doi.org/10.1111/gcb.13274

Cabré, A., Shields, D., Marinov, I., & Kostadinov, T. S. (2016). Phenology of Size-Partitioned Phytoplankton Carbon-Biomass from Ocean Color Remote Sensing and CMIP5 Models. *Frontiers in Marine Science*, *3*. https://doi.org/10.3389/fmars.2016.00039

Caracciolo, M., Beaugrand, G., Hélaouët, P., Gevaert, F., Edwards, M., Lizon, F., Kléparski, L., & Goberville, E. (2021). Annual phytoplankton succession results from niche-environment interaction. *Journal of Plankton Research*, *43*(1), 85–102. https://doi.org/10.1093/plankt/fbaa060

722 Chivers, W. J., Edwards, M., & Hays, G. C. (2020). Phenological shuffling of major marine
723 phytoplankton groups over the last six decades. *Diversity and Distributions*, *26*(5), 536–548.
724 https://doi.org/10.1111/ddi.13028
725 Cushing, D. H. (1990). Plankton Production and Year-class Strength in Fish Populations: An Update of
726 the Match/Mismatch Hypothesis. *Advances in Marine Biology*, *26*, 249–293.
727 https://doi.org/10.1016/S0065-2881(08)60202-3
728 Dutkiewicz, S., Cermeno, P., Jahn, O., Follows, M. J., Hickman, A. E., Taniguchi, D. A. A., & Ward, B. A.
729 (2020). Dimensions of marine phytoplankton diversity. *Biogeosciences*, *17*(3), 609–634.
730 https://doi.org/10.5194/bg-17-609-2020
731 Dutkiewicz, S., Scott, J. R., & Follows, M. J. (2013). Winners and losers: Ecological and biogeochemical
732 changes in a warming ocean. *Global Biogeochemical Cycles*, *27*(2), 463–477.
733 https://doi.org/10.1002/gbc.20042
734 Dybwad, C., Assmy, P., Olsen, L. M., Peeken, I., Nikolopoulos, A., Krumpen, T., Randelhoff, A., Tatarek,
735 A., Wiktor, J. M., & Reigstad, M. (2021). Carbon Export in the Seasonal Sea Ice Zone North of
736 Svalbard from Winter to Late Summer. *Frontiers in Marine Science*, *7*, 525800.
737 https://doi.org/10.3389/fmars.2020.525800
738 Edwards, M., Beaugrand, G., Kléparski, L., Helaouët, P., & Reid, P. C. (2022). Climate variability and
739 multi-decadal diatom abundance in the Northeast Atlantic. *Communications Earth &*
740 *Environment*, *3*, 162. https://doi.org/ttps://doi.org/10.1038/s43247-022-00492-9
741 Edwards, M., Beaugrand, G., Reid, P. C., Rowden, A. A., & Jones, M. B. (2002). Ocean climate
742 anomalies and the ecology of the North Sea. *Marine Ecology Progress Series*, *239*, 1–10.
743 https://doi.org/10.3354/meps239001
744 Edwards, M., & Richardson, A. J. (2004). Impact of climate change on marine pelagic phenology and
745 trophic mismatch. *Nature*, *430*(7002), 881–884. https://doi.org/10.1038/nature02808
746 Eyring, V., Bony, S., Meehl, G. A., Senior, C. A., Stevens, B., Stouffer, R. J., & Taylor, K. E. (2016).
747 Overview of the Coupled Model Intercomparison Project Phase 6 (CMIP6) experimental

748 design and organization. *Geoscientific Model Development*, *9*(5), 1937–1958.
749 https://doi.org/10.5194/gmd-9-1937-2016
750 Field, C. B., Behrenfeld, M. J., Randerson, J. T., & Falkowski, P. G. (1998). Primary Production of the
751 Biosphere: Integrating Terrestrial and Oceanic Components. *Science*, *281*, 237–240.
752 Friedland, K. D., Mouw, C. B., Asch, R. G., Ferreira, A. S. A., Henson, S. A., Hyde, K. J. W., Morse, R. E.,
753 Thomas, A. C., & Brady, D. C. (2018). Phenology and time series trends of the dominant
754 seasonal phytoplankton bloom across global scales. *Global Ecology and Biogeography*, *27*(5),
755 551–569. https://doi.org/10.1111/geb.12717
756 Fu, W., Randerson, J. T., & Moore, J. K. (2016). Climate change impacts on net primary production
757 (NPP) and export production (EP) regulated by increasing stratification and phytoplankton
758 communitystructure in the CMIP5 models. *Biogeosciences*, *13*(18), 5151–5170.
759 https://doi.org/10.5194/bg-13-5151-2016
760 Gause, G. F. (1934). *The struggle for existence* (Williams and Wilkins.).
761 Helaouët, P., & Beaugrand, G. (2007). Macroecology of *Calanus finmarchicus* and *C. helgolandicus* in
762 the North Atlantic Ocean and adjacent seas. *Marine Ecology Progress Series*, *345*, 147–165.
763 https://doi.org/10.3354/meps06775
764 Henson, S. A., Cole, H., Beaulieu, C., & Yool, A. (2013). The impact of global warming on seasonality of
765 ocean primary production. *Biogeosciences*, *10*, 4357–4369. https://doi.org/10.5194/bg-10-
766 4357-2013
767 Henson, S. A., Cole, H. S., Hopkins, J., Martin, A. P., & Yool, A. (2018). Detection of climate change-
768 driven trends in phytoplankton phenology. *Global Change Biology*, *24*, e101–e111.
769 https://doi.org/DOI: 10.1111/gcb.13886
770 Henson, S. A., Lampitt, R., & Johns, D. (2012). Variability in phytoplankton community structure in
771 response to the North Atlantic Oscillation and implications for organic carbon flux. *Limnology*
772 *and Oceanography*, *57*(6), 1591–1601. https://doi.org/10.4319/lo.2012.57.6.1591

Henson, S. A., Laufkötter, C., Leung, S., Giering, S. L. C., Palevsky, H. I., & Cavan, E. L. (2022). Uncertain response of ocean biological carbon export in a changing world. *Nature Geoscience*, *15*(4), 248–254. https://doi.org/10.1038/s41561-022-00927-0

Hutchinson, G. E. (1957). Concluding remarks. *Cold Spring Harbor Symposia on Quantitative Biology*, *22*, 415–427.

Hutchinson, G. E. (1978). *An introduction to population ecology* (Yale University Press).

IPCC. (2019). Technical Summary. In D. C. Roberts, H. O. Pörtner, V. Masson-Delmotte, P. Zhai, E. Poloczanska, K. Mintenbeck, M. Tignor, A. Alegria, M. Nicolai, A. Okem, J. Petzold, B. Rama, & N. M. Weyer (Eds.), *IPCC Special Report on the Ocean and Cryosphere in a Changing Climate* (pp. 39–69). Cambridge University Press.

Irwin, A. J., Nelles, A. M., & Finkel, Z. V. (2012). Phytoplankton niches estimated from field data. *Limnology and Oceanography*, *57*(3), 787–797. https://doi.org/10.4319/lo.2012.57.3.0787

Jonas, T. D., Walne, A. W., Beaugrand, G., Gregory, L., & Hays, G. C. (2004). The volume of water filtered by a Continuous Plankton Recorder sample: The effect of ship speed. *Journal of Plankton Research*, *26*(12), 1499–1506. https://doi.org/10.1093/plankt/fbh137

Karp-Boss, L., & Boss, E. (2016). The Elongated, the Squat and the Spherical: Selective Pressures for Phytoplankton Shape. In P. M. Glibert & T. M. Kana (Eds.), *Aquatic Microbial Ecology and Biogeochemistry: A Dual Perspective* (pp. 25–34). Springer International Publishing. https://doi.org/10.1007/978-3-319-30259-1_3

Kemp, A. E. S., & Villareal, T. A. (2013). High diatom production and export in stratified waters – A potential negative feedback to global warming. *Progress in Oceanography*, *119*, 4–23. https://doi.org/10.1016/j.pocean.2013.06.004

Kemp, A. E. S., & Villareal, T. A. (2018). The case of the diatoms and the muddled mandalas: Time to recognize diatom adaptations to stratified waters. *Progress in Oceanography*, *167*, 138–149. https://doi.org/10.1016/j.pocean.2018.08.002

798 Kléparski, L., Beaugrand, G., Edwards, M., Schmitt, F. G., Kirby, R. R., Breton, E., Gevaert, F., &
799 Maniez, E. (2022). Morphological traits, niche-environment interaction and temporal
800 changes in diatoms. *Progress in Oceanography*, *201*, 102747.
801 https://doi.org/10.1016/j.pocean.2022.102747
802 Kwiatkowski, L., Torres, O., Bopp, L., Aumont, O., Chamberlain, M., Christian, J. R., Dunne, J. P.,
803 Gehlen, M., Ilyina, T., John, J. G., Lenton, A., Li, H., Lovenduski, N. S., Orr, J. C., Palmieri, J.,
804 Santana-Falcón, Y., Schwinger, J., Séférian, R., Stock, C. A., … Ziehn, T. (2020). Twenty-first
805 century ocean warming, acidification, deoxygenation, and upper-ocean nutrient and primary
806 production decline from CMIP6 model projections. *Biogeosciences*, *17*(13), 3439–3470.
807 https://doi.org/10.5194/bg-17-3439-2020
808 Lewandowska, A., & Sommer, U. (2010). Climate change and the spring bloom: A mesocosm study on
809 the influence of light and temperature on phytoplankton and mesozooplankton. *Marine*
810 *Ecology Progress Series*, *405*, 101–111. https://doi.org/10.3354/meps08520
811 Litchman, E., Edwards, K. F., Klausmeier, C. A., & Thomas, M. K. (2012). Phytoplankton niches, traits
812 and eco-evolutionary responses to global environmental change. *Marine Ecology Progress*
813 *Series*, *470*, 235–248. https://doi.org/doi: 10.3354/meps09912
814 Litchman, E., & Klausmeier, C. A. (2008). Trait-Based Community Ecology of Phytoplankton. *Annual*
815 *Review of Ecology, Evolution, and Systematics*, *39*(1), 615–639.
816 Litchman, E., Klausmeier, C. A., Schofield, O. M., & Falkowski, P. G. (2007). The role of functional
817 traits and trade-offs in structuring phytoplankton communities: Scaling from cellular to
818 ecosystem level. *Ecology Letters*, *10*(12), 1170–1181. https://doi.org/10.1111/j.1461-
819 0248.2007.01117.x
820 Lürling, M. (2021). Grazing resistance in phytoplankton. *Hydrobiologia*, *848*(1), 237–249.
821 https://doi.org/10.1007/s10750-020-04370-3
822 Mannocci, L., Boustany, A. M., Roberts, J. J., Palacios, D. M., Dunn, D. C., Halpin, P. N., Viehman, S.,
823 Moxley, J., Cleary, J., Bailey, H., Bograd, S. J., Becker, E. A., Gardner, B., Hartog, J. R., Hazen, E.

L., Ferguson, M. C., Forney, K. A., Kinlan, B. P., Oliver, M. J., … Winship, A. J. (2017). Temporal resolutions in species distribution models of highly mobile marine animals: Recommendations for ecologists and managers. *Diversity and Distributions*, *23*(10), 1098–1109. https://doi.org/10.1111/ddi.12609

Margalef, R. (1978). Life-forms of phytoplankton as survival alternatives in an unstable environment. *Oceanologica Acta*, *1*(4), 493–509.

Marinov, I., Doney, S. C., & Lima, I. D. (2010). Response of ocean phytoplankton community structure to climate change over the 21st century: Partitioning the effects of nutrients, temperature and light. *Biogeosciences*, *7*, 3941–3959. https://doi.org/10.5194/bg-7-3941-2010

Martin, T. L., & Huey, R. B. (2008). Why "Suboptimal" Is Optimal: Jensen's Inequality and Ectotherm Thermal Preferences. *The American Naturalist*, *171*(3), E102–E118. https://doi.org/10.1086/527502

Miller, C. B. (2004). *Biological Oceanography*. Blackwell Science Ltd.

Naselli-Flores, L., Zohary, T., & Padisák, J. (2021). Life in suspension and its impact on phytoplankton morphology: An homage to Colin S. Reynolds. *Hydrobiologia*, *848*, 7–30. https://doi.org/10.1007/s10750-020-04217-x

O'Neill, B. C., Kriegler, E., Ebi, K. L., Kemp-Benedict, E., Riahi, K., Rothman, D. S., van Ruijven, B. J., van Vuuren, D. P., Birkmann, J., Kok, K., Levy, M., & Solecki, W. (2017). The roads ahead: Narratives for shared socioeconomic pathways describing world futures in the 21st century. *Global Environmental Change*, *42*, 169–180. https://doi.org/10.1016/j.gloenvcha.2015.01.004

O'Neill, B. C., Tebaldi, C., van Vuuren, D. P., Eyring, V., Friedlingstein, P., Hurtt, G., Knutti, R., Kriegler, E., Lamarque, J., Lowe, J., Meehl, G. A., Moss, R., Riahi, K., & Sanderson, B. M. (2016). The Scenario Model Intercomparison Project (ScenarioMIP) for CMIP6. *Geoscientific Model Development*, *9*(9), 3461–3482. https://doi.org/10.5194/gmd-9-3461-2016

849 Padisak, J., Soroczki-Pinter, E., & Rezner, Z. (2003). Sinking properties of some phytoplankton shapes
850 and the relation of form resistance to morphological diversity of plankton – an experimental
851 study. *Hydrobiologia*, *500*, 243–257.
852 Pančić, M., & Kiørboe, T. (2018). Phytoplankton defence mechanisms: Traits and trade-offs:
853 Defensive traits and trade-offs. *Biological Reviews*, *93*(2), 1269–1303.
854 https://doi.org/10.1111/brv.12395
855 Passow, U., & Carlson, C. A. (2012). The biological pump in a high CO2 world. *Marine Ecology*
856 *Progress Series*, *470*, 249–271. https://doi.org/10.3354/meps09985
857 Poloczanska, E. S., Brown, C. J., Sydeman, W. J., Kiessling, W., Schoeman, D. S., Moore, P. J., Brander,
858 K., Bruno, J. F., Buckley, L. B., Burrows, M. T., Duarte, C. M., Halpern, B. S., Holding, J., Kappel,
859 C. V., O'Connor, M. I., Pandolfi, J. M., Parmesan, C., Schwing, F., Thompson, S. A., &
860 Richardson, A. J. (2013). Global imprint of climate change on marine life. *Nature Climate*
861 *Change*, *3*(10), 919–925. https://doi.org/10.1038/nclimate1958
862 Pulliam, H. R. (2000). On the relationship between niche and distribution. *Ecology Letters*, *3*(4), 349–
863 361. https://doi.org/10.1046/j.1461-0248.2000.00143.x
864 Raven, J. A., & Waite, A. M. (2004). The evolution of silicification in diatoms: Inescapable sinking and
865 sinking as escape? *New Phytologist*, *162*(1), 45–61. https://doi.org/10.1111/j.1469-
866 8137.2004.01022.x
867 Reid, P. C., Colebrook, J. M., Matthews, J. B. L., Aiken, J., & Continuous Plankton Recorder Team.
868 (2003). The Continuous Plankton Recorder: Concepts and history, from Plankton Indicator to
869 undulating recorders. *Progress in Oceanography*, *58*(2–4), 117–173.
870 https://doi.org/10.1016/j.pocean.2003.08.002
871 Richardson, A. J., Walne, A. W., John, A. W. G., Jonas, T. D., Lindley, J. A., Sims, D. W., Stevens, D., &
872 Witt, M. (2006). Using continuous plankton recorder data. *Progress in Oceanography*, *68*(1),
873 27–74. https://doi.org/10.1016/j.pocean.2005.09.011

874 Ryabov, A., Kerimoglu, O., Litchman, E., Olenina, I., Roselli, L., Basset, A., Stanca, E., & Blasius, B.
875 (2020). *Shape matters: The relationship between cell geometry and diversity in phytoplankton*
876 [Preprint]. Ecology. https://doi.org/10.1101/2020.02.06.937219
877 Séférian, R., Berthet, S., Yool, A., Palmiéri, J., Bopp, L., Tagliabue, A., Kwiatkowski, L., Aumont, O.,
878 Christian, J., Dunne, J., Gehlen, M., Ilyina, T., John, J. G., Li, H., Long, M. C., Luo, J. Y., Nakano,
879 H., Romanou, A., Schwinger, J., … Yamamoto, A. (2020). Tracking Improvement in Simulated
880 Marine Biogeochemistry Between CMIP5 and CMIP6. *Current Climate Change Reports*, *6*(3),
881 95–119. https://doi.org/10.1007/s40641-020-00160-0
882 Smayda, T. (1970). The suspension and sinking of phytoplankton in the sea. *Oceanography and*
883 *Marine Biology - An Annual Review*, *8*, 353–414.
884 Smetacek, V. (1985). Role of sinking in diatom life-history cycles: Ecological, evolutionary and
885 geological significance. *Marine Biology*, *84*, 239–251.
886 Soberon, J., & Nakamura, M. (2009). Niches and distributional areas: Concepts, methods, and
887 assumptions. *Proceedings of the National Academy of Sciences*, *106*(Supplement_2), 19644–
888 19650. https://doi.org/10.1073/pnas.0901637106
889 Sournia, A. (1982). Form and function in marine phytoplankton. *Biological Reviews*, *57*, 347–394.
890 Stock, C. A., Alexander, M. A., Bond, N. A., Brander, K. M., Cheung, W. W. L., Curchitser, E. N.,
891 Delworth, T. L., Dunne, J. P., Griffies, S. M., Haltuch, M. A., Hare, J. A., Hollowed, A. B.,
892 Lehodey, P., Levin, S. A., Link, J. S., Rose, K. A., Rykaczewski, R. R., Sarmiento, J. L., Stouffer,
893 R., … Werner, F. E. (2011). On the use of IPCC-class models to assess the impact of climate on
894 Living Marine Resources. *Progress in Oceanography*, *88*, 1–27.
895 https://doi.org/10.1016/j.pocean.2010.09.001
896 Straile, D., Kerimoglu, O., & Peeters, F. (2015). Trophic mismatch requires seasonal heterogeneity of
897 warming. *Ecology*, *96*(10), 2794–2805. https://doi.org/10.1890/14-0839.1

898 Taucher, J., & Oschlies, A. (2011). Can we predict the direction of marine primary production change
899 under global warming? *Geophysical Research Letters*, *38*, L02603.
900 https://doi.org/10.1029/2010GL045934
901 Thackeray, S. J., Henrys, P. A., Hemming, D., Bell, J. R., Botham, M. S., Burthe, S., Helaouet, P., Johns,
902 D. G., Jones, I. D., Leech, D. I., Mackay, E. B., Massimino, D., Atkinson, S., Bacon, P. J.,
903 Brereton, T. M., Carvalho, L., Clutton-Brock, T. H., Duck, C., Edwards, M., … Wanless, S.
904 (2016). Phenological sensitivity to climate across taxa and trophic levels. *Nature*, *535*(7611),
905 241–245. https://doi.org/10.1038/nature18608
906 Thomas, M. K., Kremer, C. T., Klausmeier, C. A., & Litchman, E. (2012). A Global Pattern of Thermal
907 Adaptation in Marine Phytoplankton. *Science*, *338*(6110), 1085–1088.
908 https://doi.org/10.1126/science.1224836
909 Tréguer, P., Bowler, C., Moriceau, B., Dutkiewicz, S., Gehlen, M., Aumont, O., Bittner, L., Dugdale, R.,
910 Finkel, Z., Iudicone, D., Jahn, O., Guidi, L., Lasbleiz, M., Leblanc, K., Levy, M., & Pondaven, P.
911 (2018). Influence of diatom diversity on the ocean biological carbon pump. *Nature*
912 *Geoscience*, *11*(1), 27–37. https://doi.org/10.1038/s41561-017-0028-x
913 van der Spoel, S. (1994). The basis for boundaries in pelagic biogeography. *Progress in Oceanography*,
914 *34*(2–3), 121–133. https://doi.org/10.1016/0079-6611(94)90005-1
915 Ward, B. A., & Follows, M. J. (2016). Marine mixotrophy increases trophic transfer efficiency, mean
916 organism size, and vertical carbon flux. *Proceedings of the National Academy of Sciences*,
917 *113*(11), 2958–2963. https://doi.org/10.1073/pnas.1517118113
918 Warner, A. J., & Hays, G. C. (1994). Sampling by the continuous plankton recorder survey. *Progress in*
919 *Oceanography*, *34*(2–3), 237–256. https://doi.org/10.1016/0079-6611(94)90011-6
920 Winder, M., & Schindler, D. E. (2004). Climate change uncouples trophic interactions in an aquatic
921 ecosystem. *Ecology*, *85*(8), 2100–2106. https://doi.org/10.1890/04-0151
922 Yamaguchi, R., Rodgers, K. B., Stein, K. J., Timmermann, A., Schlunegger, S., Bianchi, D., Dunne, J. P.,
923 & Slater, R. D. (2022). Trophic level decoupling drives future change in phytoplankton bloom

924 phenology. *Nature Climate Change*, *12*, 469–476. https://doi.org/10.1038/s41558-022-
925 01353-1

926
927
928
929
930
931
932
933
934
935

936 **Figures**

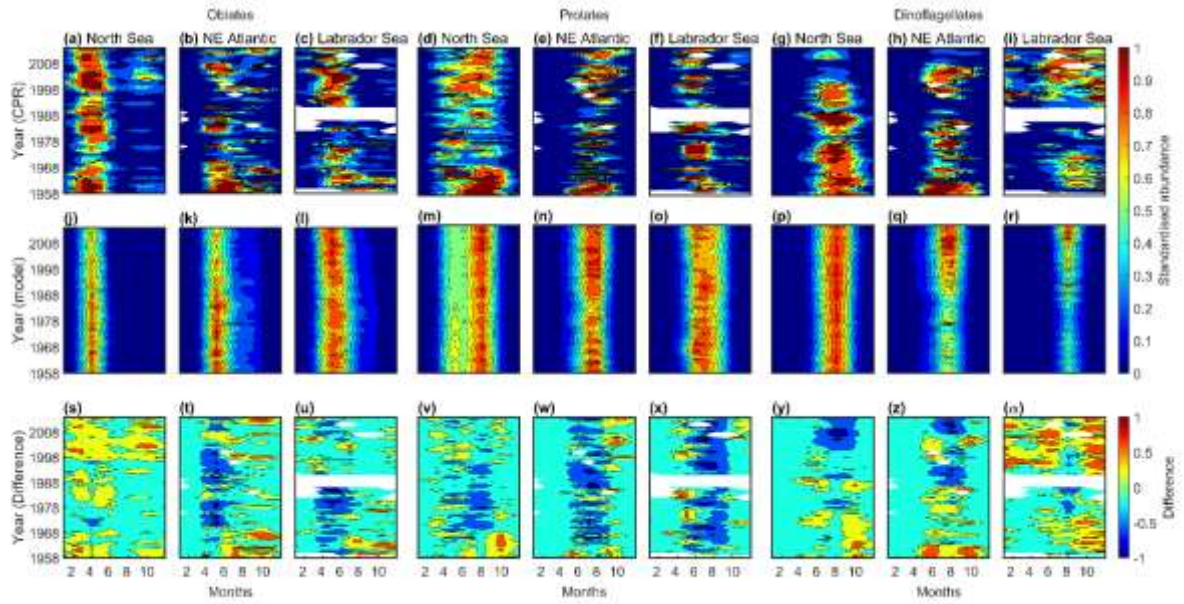

937
938 **Figure 1.**
939
940
941
942
943

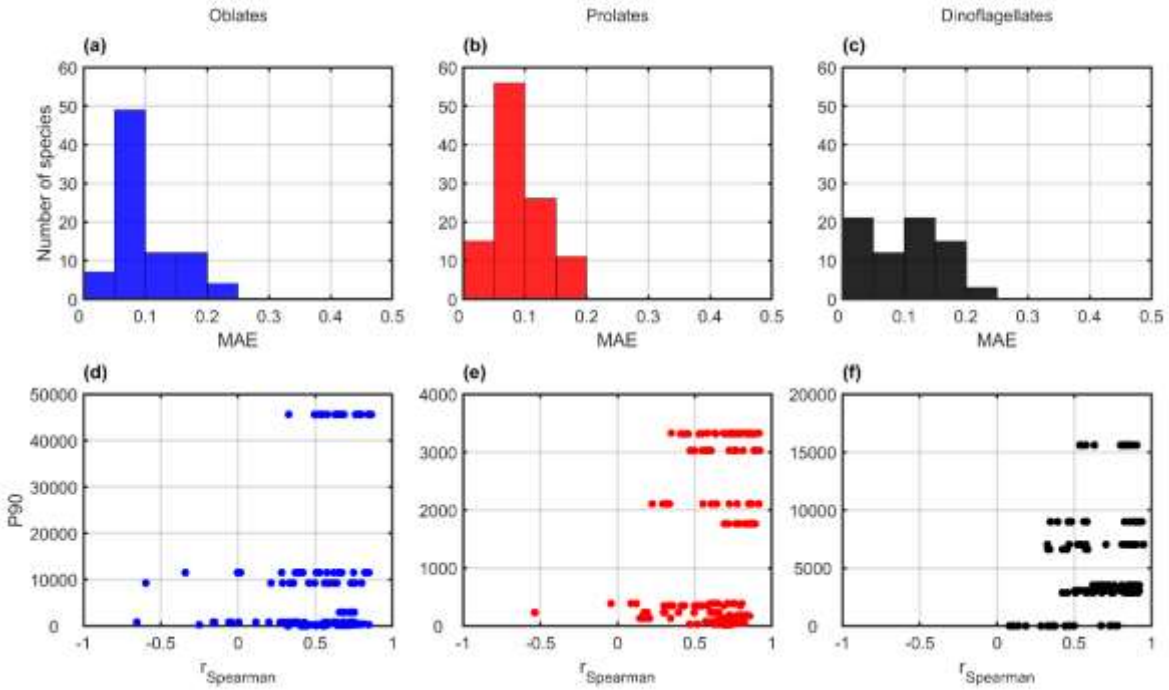

Figure 2.

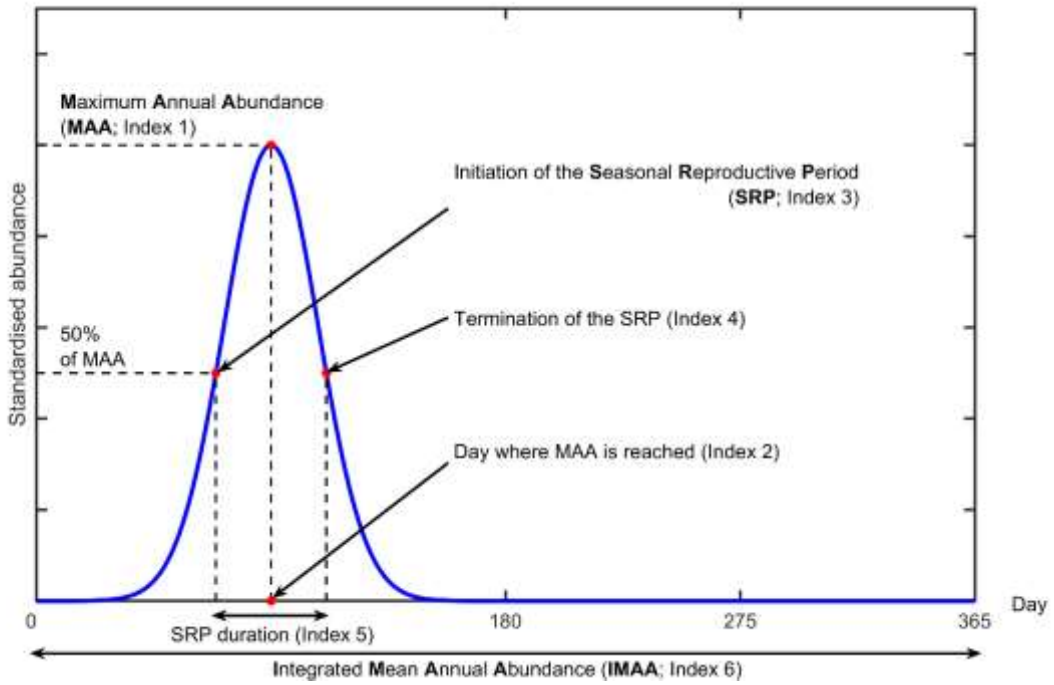

Figure 3.

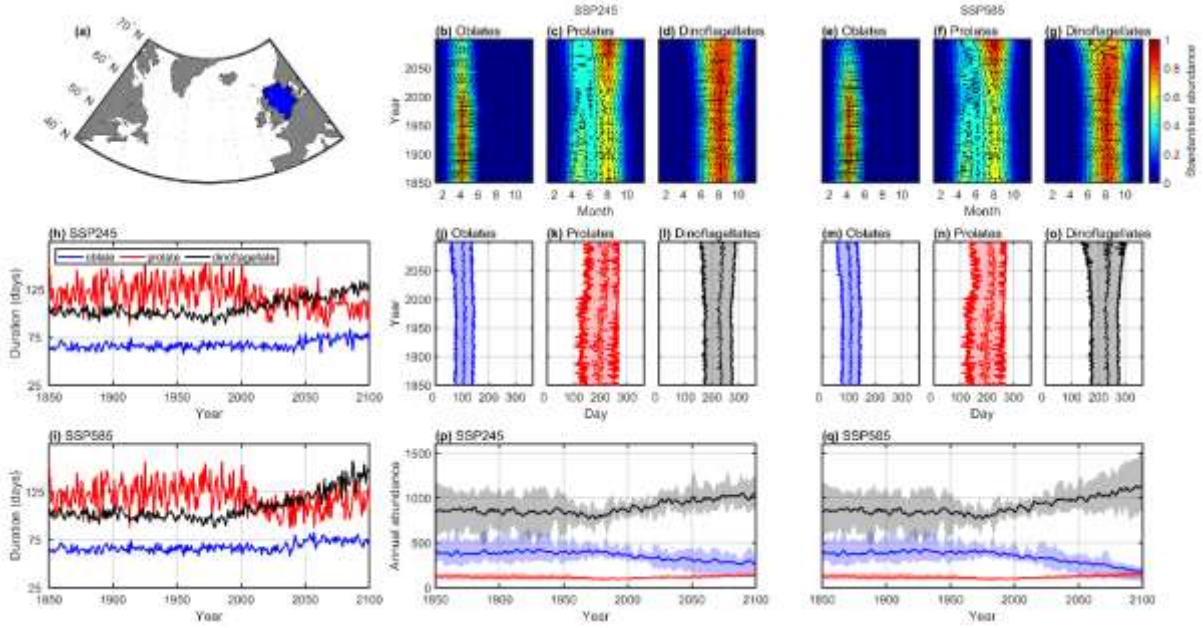

Figure 4.

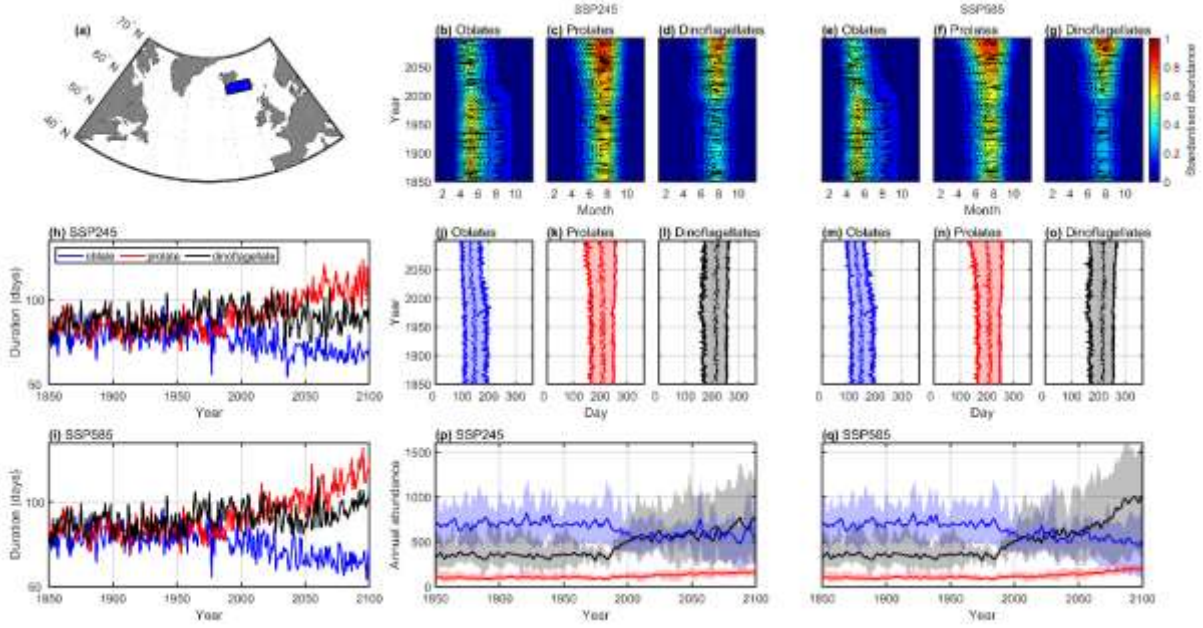

Figure 5.

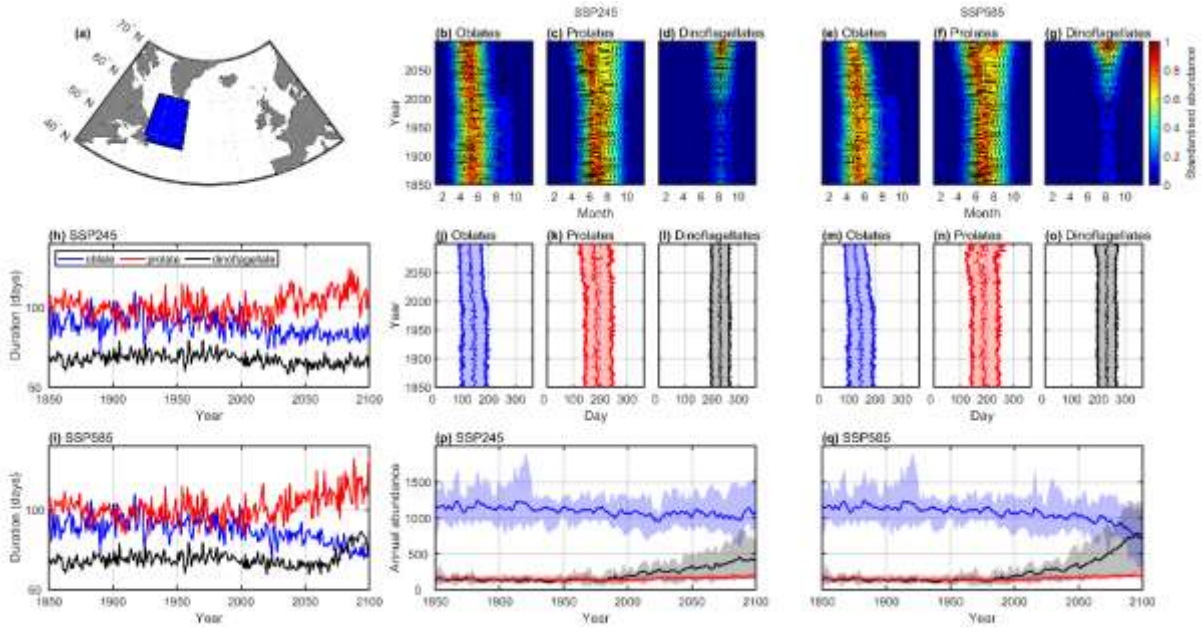

Figure 6.

Figure 1. Comparisons between observed and modelled long-term monthly abundance of the three taxonomic groups (oblates, prolates and dinoflagellates). (**a**-**i**) Long-term changes in the monthly abundance of (**a**-**c**) oblates, (**d**-**f**) prolates and (**g**-**i**) dinoflagellates in the North Sea (**a**, **d** and **g**), the North-East Atlantic (**b**, **e** and **h**) and the Labrador Sea (**c**, **f** and **i**). (**j**-**r**) Modelled long-term changes in the monthly abundance of (**j**-**l**) oblates, (**m**-**o**) prolates and (**p**-**r**) dinoflagellates in the North Sea (**j**, **m** and **p**), the North-East Atlantic (**k**, **n** and **q**) and the Labrador Sea (**l**, **o** and **r**). Differences between observed and modelled mean monthly abundance of (**s**-**u**) oblates, (**v**-**x**) prolates and (**y**-**α**) dinoflagellates in the North Sea (**s**, **v** and **y**), the North-East Atlantic (**t**, **w** and **z**) and the Labrador Sea (**u**, **x** and **α**). In **a**-**r**, colours denote the mean monthly observed or modelled abundance of a taxonomic group. The abundance in each panel was standardised between 0 and 1 for comparison purpose (Materials and Methods). Spearman correlation coefficients between observed and modelled abundance are displayed in Table 1. In **s**-**α**, colours denote the difference between observed and modelled abundance, red and blue colours indicating an underestimation and an overestimation of the modelled abundance, respectively. Modelled abundances are the average based on the six Earth System Models (ESMs).

Figure 2. Model performance. (**a**-**c**) Distribution of the Mean Absolute Errors (MAEs) calculated between observed and modelled abundances of each species/taxa for (**a**) oblates (blue bars), (**b**) prolates (red bars) and (**c**) dinoflagellates (black bars) in the three oceanic regions. (**d**-**f**) Relationships between the Spearman rank correlation ($r_{Spearman}$) calculated between the observed and the modelled abundances, and the corresponding 90th percentile of the abundance (P90; see Supplementary Table S1) values for (**d**) oblates (blue dots), (**e**) prolates (red dots) and (**f**) dinoflagellates (black dots) in the three oceanic regions. Displayed MAEs and Spearman rank correlations were calculated for each Earth

System Model (ESM) (see Supplementary Tables S2-5). Comparison between the modelled abundance forced by the six ESMs and the observed abundance by the Continuous Plankton Recorder (CPR) survey are shown in Supplementary Animations S1-3. Mean monthly observed and predicted standardised abundances of the three taxonomic groups in the three oceanic regions are shown in Figure 1.

Figure 3. Theoretical diagram explaining graphically the six phenological indices used in this study. Six phenological indices were defined: the Maximum Annual Abundance (MAA; Index 1), the day where MAA is reached (Index 2), the initiation (Index 3) and the termination (Index 4) of the Seasonal Reproductive Period (SRP), i.e., the first and the last days where the abundance is ≥50% of MAA, the seasonal duration (Index 5), i.e., the number of consecutive days where abundance is ≥ 50% of MAA, and the Integrated Mean Annual Abundance (IMAA; Index 6).

Figure 4. Modelled long-term phenological changes of diatoms and dinoflagellates in the North Sea (1850-2100). (**a**) Spatial distribution of Continuous Plankton Recorder (CPR) survey sampling. (**b**-**g**) Long-term monthly changes in the standardised abundance of (**b** and **e**) oblates, (**c** and **f**) prolates and (**d** and **g**) dinoflagellates for scenarios (**b**-**d**) SSP2-4.5 and (**e**-**g**) SSP5-8.5. Each panel was standardised between 0 and 1. Colours denote the mean monthly standardised abundance of a taxonomic group. (**h**-**i**) Long-term annual changes in phenology duration for scenarios (**h**) SSP2-4.5 and (**i**) SSP5-8.5. (**j**-**o**) Long-term changes in the initiation and termination of the Seasonal Reproductive Period (SRP) for (**j** and **m**) oblates, (**k** and **n**) prolates and (**l** and **o**) dinoflagellates. In each panel, the first and last tick line denotes the initiation and the termination day of the SRP. Shading denotes the duration of the SRP and the dotted line displays the day where Maximum Annual Abundance (MAA) is reached. (**p**-**q**) Long-term changes in Integrated Mean Annual Abundance (IMAA; cell per CPR sample) for scenarios (**p**) SSP2-4.5 and (**q**) SSP5-8.5. The shade denotes the minimum and maximum mean abundance estimated from the environmental variables originating from the six Earth System Models (ESMs). In **h**-**q** oblates are in blue, prolates in red and dinoflagellates in black. In (**b**-**q**), each index corresponds to the mean of the six ESMs. The meaning of the six phenological indices is summarised in Figure 3.

Figure 5. Modelled long-term phenological changes of diatoms and dinoflagellates in the North-East Atlantic (1850-2100). (**a**) Spatial distribution of Continuous Plankton Recorder (CPR) sampling. (**b**-**g**) Long-term monthly changes in the standardised abundance of (**b** and **e**) oblates, (**c** and **f**) prolates and (**d** and **g**) dinoflagellates for scenarios (**b**-**d**) SSP2-4.5 and (**e**-**g**) SSP5-8.5. Each panel was standardised between 0 and 1. Colours denote the mean monthly standardised abundance of a taxonomic group. (**h**-**i**) Long-term annual changes in phenology duration for scenarios (**h**) SSP2-4.5 and (**i**) SSP5-8.5. (**j**-**o**) Long-term changes in the initiation and termination of the Seasonal Reproductive Period (SRP) for (**j** and **m**) oblates, (**k** and **n**) prolates and (**l** and **o**) dinoflagellates. In each panel, the first and last tick line denotes the initiation and the termination day of the SRP. Shading denotes the duration of the SRP and the dotted line displays the day where Maximum Annual Abundance (MAA) is reached. (**p**-**q**) Long-term changes in Integrated Mean Annual Abundance (IMAA; cell per CPR sample) for scenarios (**p**) SSP2-4.5 and (**q**) SSP5-8.5. The shade denotes the minimum and maximum mean abundance estimated from the environmental variables originating from the six Earth System Models (ESMs). In **h**-**q** oblates are in blue, prolates in red and dinoflagellates in black. In (**b**-**q**), each index corresponds to the mean of the six ESMs. The meaning of the six phenological indices is summarised in Figure 3.

Figure 6. Modelled long-term phenological changes of diatoms and dinoflagellates in the Labrador Sea (1850-2100). (**a**) Spatial distribution of Continuous Plankton Recorder (CPR) sampling. (**b**-**g**) Long-term monthly changes in the standardised abundance of (**b** and **e**) oblates, (**c** and **f**) prolates and (**d** and **g**) dinoflagellates for scenarios (**b**-**d**) SSP2-4.5 and (**e**-**g**) SSP5-8.5. Each panel was standardised between 0 and 1. Colours denote the mean monthly standardised abundance of a taxonomic group. (**h**-**i**) Long-term annual changes in phenology duration for scenarios (**h**) SSP2-4.5 and (**i**) SSP5-8.5. (**j**-**o**) Long-term changes in the initiation and termination of the Seasonal Reproductive Period (SRP) for (**j** and **m**) oblates, (**k** and **n**) prolates and (**l** and **o**) dinoflagellates. In each panel, the first and last tick line denotes the initiation and the termination day of the SRP. Shading denotes the duration of the SRP and the dotted line displays the day where Maximum Annual Abundance (MAA) is reached. (**p**-**q**) Long-term changes in Integrated Mean Annual Abundance (IMAA; cell per CPR sample) for scenarios (**p**) SSP2-4.5 and (**q**) SSP5-8.5. The shade denotes the minimum and maximum mean abundance estimated from the environmental variables originating from the six Earth System Models (ESMs). In **h**-**q** oblates are in blue, prolates in red and dinoflagellates in black. In (**b**-**q**), each index corresponds to the mean of the six ESMs. The meaning of the six phenological indices is summarised in Figure 3.

Table

Table 1. Spearman rank correlations between long-term changes in observed and modelled monthly abundance of the three taxonomic groups (oblates, prolates and dinoflagellates) in the three studied regions. All correlations were significant ($p<0.01$). The degree of freedom associated with each oceanic region are also indicated. Long-term monthly changes in observed and modelled abundance are displayed in Figure 1.

	North Sea	North-East Atlantic	Labrador Sea
Oblates	0.70	0.64	0.55
Prolates	0.79	0.73	0.58
Dinoflagellates	0.83	0.72	0.50
Degree of freedom	684	677	600